Chinese Chemical Letters 33 (2022) 835–841

Contents lists available at ScienceDirect

Chinese Chemical Letters

journal homepage: www.elsevier.com/locate/cclet

Enhancement of morphological and emission stability of deep-blue small molecular emitter *via* a universal side-chain coupling strategy for optoelectronic device

Ning Sun[a,1], Han Gao[a,1], Lili Sun[a,1], Jingxi An[b], Man Xu[b], Chen Sun[a], Yamin Han[a], Jinyi Lin[a,*], Jiangli Cai[a], Mingjian Ni[a], Liangliang He[a], Jinghao Yang[a], Zhoulu Wang[a,*], Lubing Bai[a], Xinwen Zhang[b], Qi Wei[a], Xuehua Ding[a,*], Chengrong Yin[a], Linghai Xie[b], Wei Huang[a,b,c,**]

[a] *Key Laboratory of Flexible Electronics (KLOFE) and Institute of Advanced Materials (IAM), Nanjing Tech University (NanjingTech), Nanjing 210000, China*
[b] *State Key Laboratory of Organic Electronics and Information Displays and Institute of Advanced Materials (IAM), Nanjing University of Posts and Telecommunications, Nanjing 210023, China*
[c] *Frontiers Science Center for Flexible Electronics (FSCFE), MIIT Key Laboratory of Flexible Electronics (KLoFE), Northwestern Polytechnical University, Xi'an 710072, China*

ARTICLE INFO

Article history:
Received 7 May 2021
Revised 27 July 2021
Accepted 30 July 2021
Available online 5 August 2021

Keywords:
Side-chain coupling
Small molecular emitter
Morphological stability
Deep-blue emission
Optoelectronic device

ABSTRACT

Film morphology of emissive layers is crucial to the performance and stability of solution-processable organic light-emitting diodes (OLEDs). Compared to the interpenetration of conjugated polymer chain, small molecular emitter with a flexible side chain always presents easily aggregation upon external treatment, and caused π-electronic coupling, which is undesirable for the efficiency and stability of deep-blue OLEDs. Herein, we proposed a side-chain coupling strategy to enhance the film morphological an emission stability of solution-processable small molecular deep-blue emitter. In contrary to "parent" MC8TPA, the crosslinkable styryl and vinyl units were introduced as ended unit at the side-chain of CmTPA and OEYTPA. Interestingly, CmTPA and OEYTPA films present a relatively stable morphology and uniform deep-blue emission after thermal annealing (160 °C) in the atmosphere, different to the discontinuous MC8TPA annealed film. Besides, compared to the CmTPA and OEYTPA ones, serious polaron formation in the MC8TPA annealed film also negative to the deep-blue emission, according to transient absorption analysis. Therefore, both CmTPA and OEYTPA annealed film obtained at 140 °C present an excellent deep-blue ASE behavior with a 445 nm, but absence for MC8TPA ones, associated with the disruption of annealed films. Finally, enhancement of device performance based on CmTPA and OEYTPA film (~40%) after thermal annealing with a similar performance curves also confirmed the assumption above. Therefore, these results also supported the effectiveness of our side-chain coupling strategy for optoelectronic applications.

In the last decades, light-emitting materials have attracted more attentions, due to their potential applications in information display and solid light [1–9]. In general, inorganic emitter always present excellent stable emission behavior and efficient luminance efficiency, associated with the intrinsic stable atomic bonds in solid states [10,11], which are enable a relatively excellent thermal morphological stability [1,8,12]. However, consideration of the relative freedom motion of C-C chemical bond (such as σ and π-bonds) [13], molecular motion of organic materials can be easily activated under external post-treatment, result into conformational transition, intermolecular rearrangement and crystallization in solid states [14–17]. Especially, these molecular wriggles are also observed in film state under thermal stimulation, such as residual thermal-energy in device fabrication, and Joule self-heating in device operation [14,18–22]. Obviously, this intermolecular aggregation caused by molecular wriggles, also induce serious electronic

* Corresponding authors.
** Corresponding author at: Key Laboratory of Flexible Electronics (KLOFE) and Institute of Advanced Materials (IAM), Nanjing Tech University (NanjingTech), Nanjing 210000, China.
E-mail addresses: iamjylin@njtech.edu.cn (J. Lin), WangZhouLu66@163.com (Z. Wang), iamxhding@njtech.edu.cn (X. Ding), wei-huang@njtech.edu.cn (W. Huang).
[1] These authors contributed equally to this work.

https://doi.org/10.1016/j.cclet.2021.07.069
1001-8417/

coupling, polaron formation, charge trapping, and exciton-exciton annihilate in the solid states, which is undesirable for deep-blue OLEDs [17,23–33]. Up to date, the steric functionalization of conjugated molecules is the most molecular design strategy to suppress this molecular motion *via* improving glass transition temperature (T_g), such as corporation of steric bulky unit, dendron groups and large cycles ring [28,29,34–37]. However, such synthetic procedures are laborious, spatial distribution of the groups is congestion, and caused low solubility [25,26,30,38–42]. What is more, insulated cyclical or large steric frameworks tend to randomly distribute in condensed structures, which significantly affect the intermolecular charge transport properties [26,34,40,42–44]. In consideration of this situation, it is urgent to establish a simple and universal molecular design principle to improve the morphological and emission stability of small molecular deep-blue emitter.

Compared to the deposited ones, solution-processable organic emitters present a series of advantages, such as low cost technology, room temperature processing and easily large-scale manufacture for the fabrication of optoelectronic devices [12,28,45–48]. In general, conjugated polymeric emitters present an excellent film solution processing ability, associated with its intrinsic viscosity induced by interchain entanglement [39,45,48]. And the small molecular emitter with a flexible substituted chain and supramolecular units is another type materials act as active layer for fabricating solution-processed optoelectronic devices [2,12,28,47]. In fact, the introduce of this flexible side chain is useful to obtain proper viscosity for improving film-forming ability [12,49], but caused low freedom energy for intermolecular rearrangement under thermal treatment, due to the small T_g, which is negative to the device performance and stability. In this regard, it is predicated that suppress molecular freedom motion is effective strategy to enhance the morphological and emission property of small molecular emitter. Previously, an efficient small deep-blue nano-emitter (MC8TPA) is obtained for deep-blue OLEDs and organic laser [50,51]. However, similar to reported small molecular emitters, our nano-molecules also present lower T_g and result into intermolecular aggregation, which is negative to device performance and stability [24,27,28,50–52]. Herein, we proposed a universal side-chain intermolecular-coupled strategy to enhance the morphological and emission behavior of MC8TPA in solid states. Compared to the freedom motion of "parent" small molecules, the chemical coupling bond between chromophore units can suppress the molecular wriggles and intermolecular aggregation. Therefore, the active vinyl groups are introduced act as the ended units of side chain at 4-position of fluorenes, CmTPA and OEYTPA, as shown in Fig. 1a. As we expected, intermolecular network present excellent morphological and deep-blue emission stability. Finally, significantly different to MC8TPA ones, the performance and emission spectra of OLEDs based CmTPA and OEYTPA annealed film are independent on the thermal annealed temperatures, also further confirmed the effectiveness of our design strategy.

Firstly, we proposed two novel organic small molecular luminescent materials, CmTPA and OEYTPA with a sterically hindered and linkable ingredient [53–55], referenced to the molecular modification of MC8TPA, which successfully synthesized *via* Suzuki cross coupling reaction (Fig. S1 in Supporting information). In order to compare the properties of the newly synthesized materials, "parent" MC8TPA was used as the reference that was investigated in our group previous study [50]. Compared with MC8TPA, double bond groups with different activities were introduced into the 4-possion of fluorene (Fig. 1b), that the styryl and vinyl units were introduced into CmTPA and OEYTPA, respectively [53,56]. Hence, whether the multi-step reaction process affects the activity of the double bond needs to take into account in the synthesis. In order to solve this issue, we redesigned the synthetic route, and the introduction of the side chain was incorporated at the last

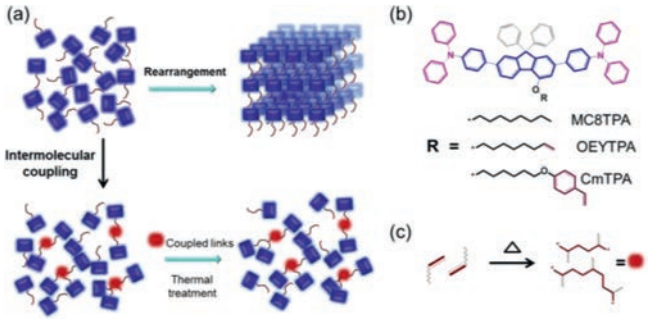

Fig. 1. Molecular-coupling design principle of our model steric deep-blue emitter. (a) Schematic representation of the suppressing freedom motion of deep-blue chromophore by the side-chain coupling strategy. Consideration of diverse molecular wriggles, small molecules are easily aggregate together under thermal treatment, which is effectively suppressed in a cross-linked network. (b) Chemical structures of MC8TPA, OEYTPA and CmTPA. Molecules can be easily coupled in the solid state by the active reaction of vinyl unit at the end of substituted side-chain in fluorenes units, which is useful to inhibit molecular rearrangement and crystallization. (c) Possible cross-linking reaction principle of vinyl unit under thermal treatment.

step (Fig. S1). The specific reaction steps are shown in Supporting information. Firstly, nuclear magnetic resonance (NMR) measurement was used here to confirm the chemical structures of the three TPA materials, as show in Fig. S2 (Supporting information). Simultaneously, three materials have an excellent solubility in organic solvents, such as toluene, tetrahydrofuran and chloroform, contribute to solution process for device fabrication. CmTPA and OEYTPA showed similar decomposition temperature (T_d), which higher than that of MC8TPA nearly 10 °C, reached up to 428 °C and 423 °C, respectively. Interestingly, the T_g of CmTPA is slightly higher than that of OEYTPA and MC8TPA as indicated by differential scanning calorimetry (DSC) (Fig. S3 in Supporting information) [50].

As we designed strategy, intermolecular coupling of OEYTPA and CmTPA materials is positive to improve their thermal stability. In order to check this assumption, we set CmTPA to explore this thermal behavior *via* cycle thermal treatment. The maximum temperature of the DSC test was controlled at 180 °C and it was carried out in a nitrogen atmosphere. The data obtained clearly show that, except for the endothermic peak in the first scan, the T_g obtained from the next few scans are lower than 140 °C (Fig. S4 in Supporting information). Interestingly, as we expected, the T_g of CmTPA powders gradually increases from 150 °C to nearly 180 °C with the increase number of scan cycles, when the maximum temperature of the DSC test was controlled at 350 °C (Fig. 2a). The T_g of MC8TPA was also tested using DSC, that the maximum temperature was controlled at 250 °C and maintained for 5 min, as shown in Fig. S5 (Supporting information). After the samples tested for DSC can be partial dissolved in DCM, which further spotted on a silica gel plate with a eluent of PE:DCM=2:1 (insert in Fig. S5). Beyond the parent one, a series of extra new points also observed for OEYTPA and CmTPA (similar to Fig. 2c), suggested the intermolecular coupling of OEYTPA, significantly different to MC8TPA ones. According to previous works [53,56], styryl and vinyl units can be active to induce intermolecular coupling under thermal treatment, which is effective to obtain cross-linked network in solid states. Of course, the reaction of styryl units is more activity than that of vinyl ones, which may cause the nano-scale morphological change after thermal treatment. Therefore, the intermolecular couple of CmTPA and OEYTPA at 4-postion of fluorene may effectively suppress molecular rearrangement and recrystallization, and easily improve thermal stability of small molecular emitters.

To identify the nature of these intermolecular coupling, temperature-dependent Fourier-transform infrared (FT-IR) spec-

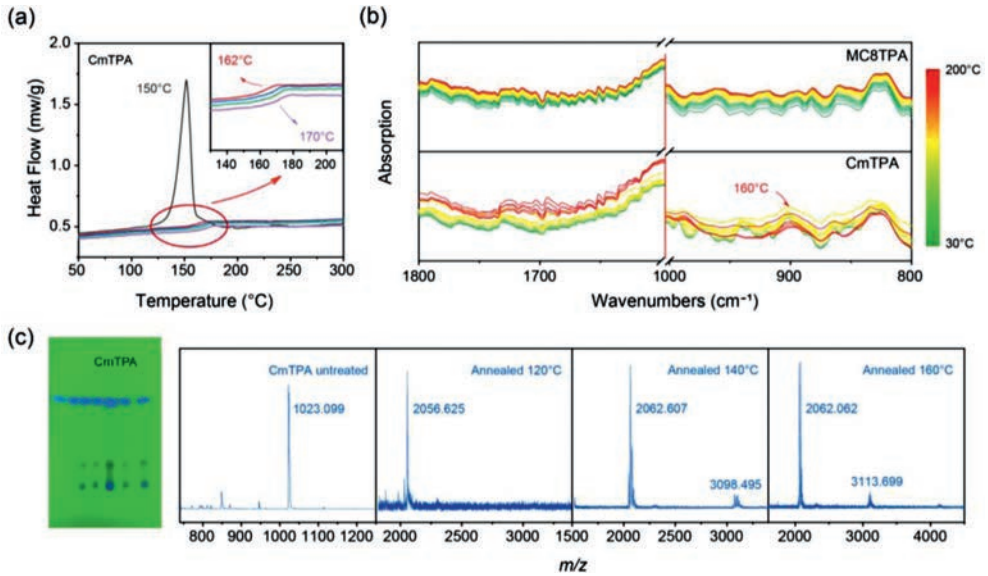

Fig. 2. Intermolecular coupling of CmTPA in solid states. (a) DSC curves of CmTPA powder in several thermal cycles. The maximum temperature of the DSC test was controlled at 350 °C. (b) Variable temperature IR curves of MC8TPA and CmTPA powders from 30 °C to 200 °C. (c) Photographs images of TLC plate after thermal-induce coupling reaction, together with the Modi-Tof data of CmTPA drop-coated film at different temperatures. The points on the TLC plate are the original solution of CmTPA and the drop films annealed at different temperatures. The drop film of CmTPA was annealed at 120, 140, 150, 160, 180 and 200 °C for 30 min, respectively.

troscopy is also introduced to explore the molecular vibration and motion of the styryl-contained side chain and mainchain backbone for CmTPA [53]. As presented in Fig. 2b, the absorbance change on the terminal styryl unit, show weaken peaks at about 1645 cm^{-1}, due to the loss of C=C stretching vibration with increasing temperature to 160 °C. Meanwhile, the out of plane swing vibration absorption peak of =C–H at about 910–905 and 995–985 cm^{-1}, which are characteristics of the terminal double bond, disappeared when temperature rose more than 160 °C yet (Fig. 2b and Fig. S6 in Supporting information), also confirmed the coupling reaction of styryl under thermal annealing. Subsequently, in order to confirm this assumption and critical coupling temperature, product structures of CmTPA after coupling reaction are systematically investigated *via* preliminary thin layer chromatography (TLC) and MALDI-TOF-MS spectrometry test. Firstly, we obtained a series of annealed drop-coated films of CmTPA after thermal treatment at 120, 140, 150, 160, 180 and 200 °C, respectively. Subsequently, the film was partial dissolved in the chloroform solvent. Finally, the pristine CmTPA solution was used as a reference one. As displayed in Fig. 2c, the drop film of CmTPA had been annealed at 120 °C for 0.5 h, and a trace amount of new material had been formed, and when the annealing temperature was gradually increased, the content of new substances generated was increasing yet, and the specific manifestation was that the new spots were gradually increasing. Combined with the further analysis of the chemical structure of CmTPA, the adjacent CmTPA end active styryl units were coupled. In this regard, the critical coupling temperature (CCT) of CmTPA is about 120 °C. Besides, MALDI-TOF-MS test was also explored here to confirm this assumption (Fig. 2c). It clearly shows that the maximum *m/z* (mass-to-charge ratio) value of the unannealed drop film is 1023, associated with the single CmTPA molecule. Interestingly, a small peak near the *m/z* of 2050 is observed in the MALDI-TOF-MS curve of the drop film of CmTPA after annealed at 120 °C for 0.5 h, suggested the dimer formation. With increasing the annealing temperatures to 140 °C, the maximum value of *m/z* also increases to 3098, confirmed obtaining CmTPA trimer, consistent with the possible cross-linking reaction principle in Fig. 1c. And there is an unobvious peak at *m/z* over 4000 for 160 °C. These data more intuitively indicated that the neighbouring CmTPA molecules are coupled during the annealing process. Meanwhile, the fraction of molecules can be coupled at higher temperature. Hence, it demonstrated that the coupling degree of adjacent CmTPA molecules is positively correlated with annealing time and temperature, that this intermolecular coupling can effectively improve morphological stability.

Subsequently, we also investigated the film morphological stability and emission behavior of three materials after thermal annealing, as present in Fig. 3. For MC8TPA materials, pristine films present a smooth and continuous states, revealed excellent film formation ability induced by the flexible side-chain substitute. Meanwhile, an efficient and uniform deep-blue emission also confirmed this assumption. However, there are series of pores observed in the annealed MC8TPA film (120 °C and 140 °C) secondary treatment under 160 °C, suggested the destruction of MC8TPA film under thermal processing, associated with the strong intermolecular rearrangement and phase transition, consistent with the DSC results. This discontinuous film morphology is seriously negative to the device performance and stability. Interestingly, similar to the discussion above, our OEYTPA and CmTPA displayed an excellent thermal stability and relative uniform emission. As displayed in Figs. 3d and g, similar to MC8TPA, OEYTPA and CmTPA pristine film had excellent film morphology, efficient and uniform deep-blue emission. As we expected, our CmTPA annealed films also present excellent deep-blue emission with uniform surface, even further secondary treatment under 160 °C, confirmed its excellent film morphological stability. Compared to MC8TPA materials, our OEYTPA had a relatively better morphological stability, but weaker than those of CmTPA, however, suggested the weaker intermolecular aggregation and crystallization, reasonably explained by the weaker reaction activity of vinyl units than those of styryl ones. Therefore, it is effectively concluded that the side intermolecular coupling of small molecules can improve the morphological and emission stability of small molecular emitter.

Generally, interchain aggregation with an electron coupling will affect the photophysical processes in the solid states [13,32,57]. Here, we further investigated the optical properties of three compounds in various states. Similar to previous work [50,51], CmTPA, OEYTPA and MC8TPA diluted solution show similar absorption

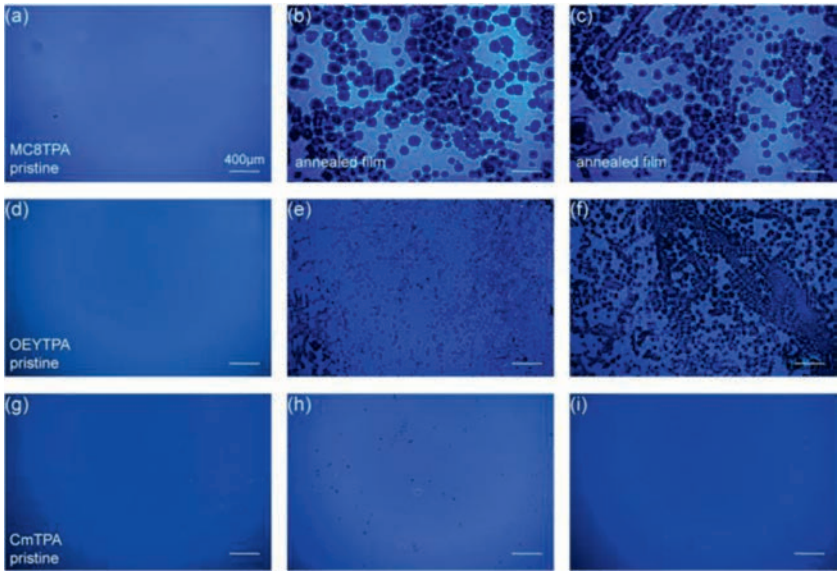

Fig. 3. Fluorescence microscope (FLM) images of MC8TPA (a-c), OEYTPA (d-f) and CmTPA (g-i) pristine film, and annealed films (obtained thermal treatment at 120 °C and 140 °C) secondary treatment under 160 °C, respectively. Scale bar is 200 nm.

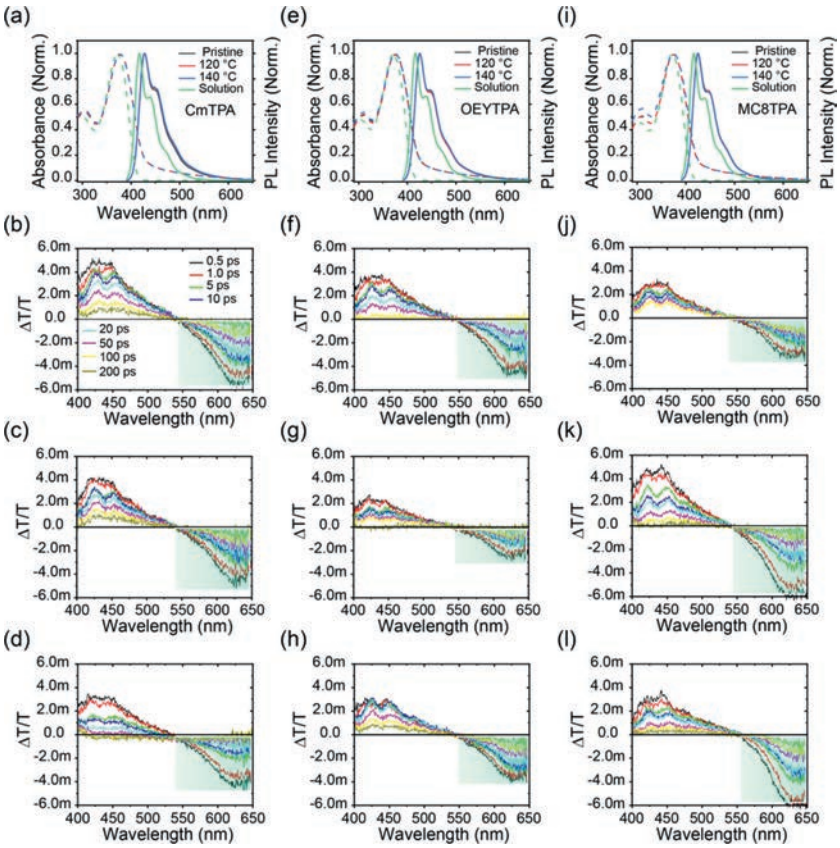

Fig. 4. Optical properties of MC8TPA, OEYTPA and CmTPA in various states. Steady absorption and PL spectra of CmTPA (a), OEYTPA (e) and MC8TPA (i) in diluted toluene solution, pristine, annealed and aged film. $\Delta T/T$ kinetics of transient absorption spectra of CmTPA (b), OEYTPA (f) and MC8TPA (j) pristine spin-coated films from toluene solution, and corresponding annealed films (obtained thermal treatment at 120 °C and 140 °C) secondary treatment under 160 °C (c and d, g and h, k and l), respectively.

peak at 372 nm as displayed in Fig. 4, associated with the similar conjugated backbone structures. Meanwhile, in light of those compounds PL spectrum of dilute solution, three feature emission peaks are observed at 417, 438 and 470 nm, which attributed to the 0-0, 0-1 and 0-2 vibronic transitions. Similar absorption spectral profile between solution and film states of CmTPA, OEYTPA and MC8TPA also confirmed no obvious aggregation in solid state [25,26,32,43]. Compared to the solution states, similar emission spectral profile with slightly red-shift of about 10 nm are observed for those three compounds pristine films. Interestingly, the annealed films of three compounds exhibit same profile with pristine films, which thermal annealed at 120 °C or 140 °C for 0.5 h,

respectively. As we expected, all three materials present the identical emission spectra, similar to the pristine ones, indicated the excellent thermal emission stability. Besides, we also explored the effect of aging processing on the photophysic property of spin-coated films [43]. Then, we kept our spin coating film with various thermal annealed temperatures in air for about 3 days to check their storage stability. As expected, our novel CmTPA and OEYTPA present identical deep-blue emission spectra for pristine ones, without any green-emission at 550 nm for aged film, as show in Fig. S7 (Supporting information). However, there is lightly weak green-band emission (500–600 nm) with long spectral tail for MC8TPA aged film. Meanwhiles, as presented in Fig. S8 (Supporting information), PL 1/e decay times of CmTPA, OEYTPA and MC8TPA are 0.281, 0.338 and 0.464 ns for pristine spin-coated film and 0.283, 0.334 and 0.428 ns for thermal annealed spin-coated film, respectively. The shorter life-time of CmTPA and OEYTPA pristine and annealed film may slightly avoid exciton trapping. What is more, the fluorescence quantum yields (Φ) of the pristine spin-coated films were 23.92% ± 5%, 29.6% ± 5% and 26.78% ± 5%, the thermal annealed spin-coated films with 120 °C were 25.69% ± 5%, 32.99% ± 5%, and 33.44% ± 5% for CmTPA, OEYTPA and MC8TPA (Table S1 in Supporting information), respectively, which were promising candidates for solid-state emissive materials in the future.

According to previous works, in fact, steady optical analysis is insensitive measures to evaluate the emission stability, especial the residual physical defect [43,58]. Subsequently, the transient absorption experiments of three materials are also performed here in various solid states, indicated the broad stimulate emission (SE) spectrum, excited states belonging exclusively to the singlet manifold and lack of sub-ps relaxation associated to exciton-exciton annihilation in OEYTPA and CmTPA annealed films than those for MC8TPA [23,24,29,30,43,59]. As displayed in Figs. 4b, f and g, both CmTPA, OEYTPA and MC8TPA pristine spin-coated films present a strong SE band with two feature peaks of 420 and 450, similar to PL spectral profile of diluted solution, associated with robust singlet manifold. However, obvious photoinduced absorption (PA) band which peaks at ~611 nm and ~644 nm for three pristine films, clarified as PAs (singlet excitons) and PAp (polaron pairs) are observed, which have quite different kinetics, which seems like the dynamic of long-lived polaron pairs [30,59]. This polaron formation is closely with the exciton-exciton annihilation, which is negative to the emission efficiency and stability of emitters [30,59]. Interestingly, CmTPA film had both stronger SE band and PA band, than those of MC8TPA, OEYTPA ones (Fig. S9 in Supporting information), also reasonably explained its lowest PLEQ. However, the intensity of PA band for MC8TPA is significantly enhanced in annealed film, both for thermal treatment at 120 °C and 140 °C. What is more, there are weaker SE band observed for MC8TPA annealed film (Fig. 4i and Fig. S9), also confirmed the formation of polaron pair caused by the intermolecular aggregation, consistent with the Fig. 3. In fact, strong light scattering by micro-scale aggregate in MC8TPA annealed film also responsible for this strong PAs band (Figs. 3b and c). In contrary, both CmTPA and OEYTPA annealed film present a relatively weak PA and strong SE band, confirmed weaker intermolecular aggregation and low exciton-exciton annihilation. In fact, OEYTPA also had a stronger comprehensive single-excitonic emission with weak exciton-exciton annihilation than those of CmTPA (Fig. 4 and Fig. S9), also indicated a robust deep-blue emission. Starting from OEYTPA, the dynamic of SE and PA band show almost perfect symmetry behavior which suggest only contribution from singlet excitons to these bands and indicate no influence comes from polaron pairs, confirmed weaker intermolecular aggregation. Unlikely, in MC8TPA annealed film, PA at 600–650 nm clearly exhibit a longer-lived component which can be ascribe as polaron pairs and will further cause more painful for the emission property. In this regard, compared to MC8TPA ones, robust emission behavior will obtain in annealed film of CmTPA and OEYTPA, which is desirable for light-emitting optoelectronic devices.

In general, amplified spontaneous emission (ASE) property of organic emitter is key parameter to evaluate the exciton behavior in solid state [30,59]. Hence, we exploited the ASE behavior of CmTPA, OEYTPA and MC8TPA pristine and annealed spin-coated film. As shown in Fig. 5, ASE spectra of three pristine films present a typical maximum peak at 445–450 nm, attributed to the 0–1 vibration transition of single molecule. MC8TPA pristine film had an ASE peak at 446 nm with a low threshold pulse energy (E^{th}_{ASE}) of 13.2 μJ/cm^2, indicated an excellent deep blue emission, consistent with the result of optical analysis. This low-threshold (9.2 μJ/cm^2)

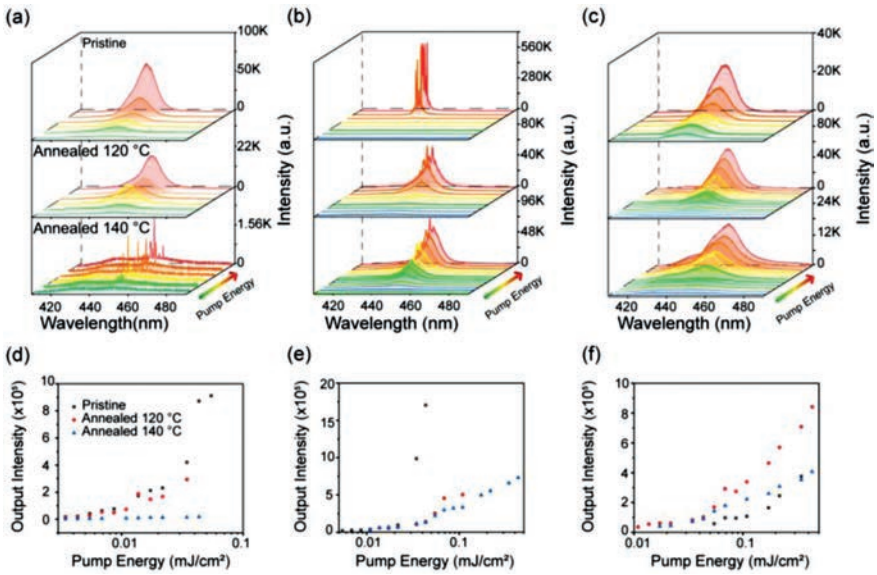

Fig. 5. ASE behavior of three compounds pristine film and annealed films. Normalized emission and ASE spectra (excited at 355 nm) of the MC8TPA (a), OEYTPA (b) and CmTPA (c) pristine films, annealed film at 120 °C and 140 °C. Corresponding ASE output intensity versus pump energy density for the MC8TPA (d), OEYTPA (e) and CmTPA (f).

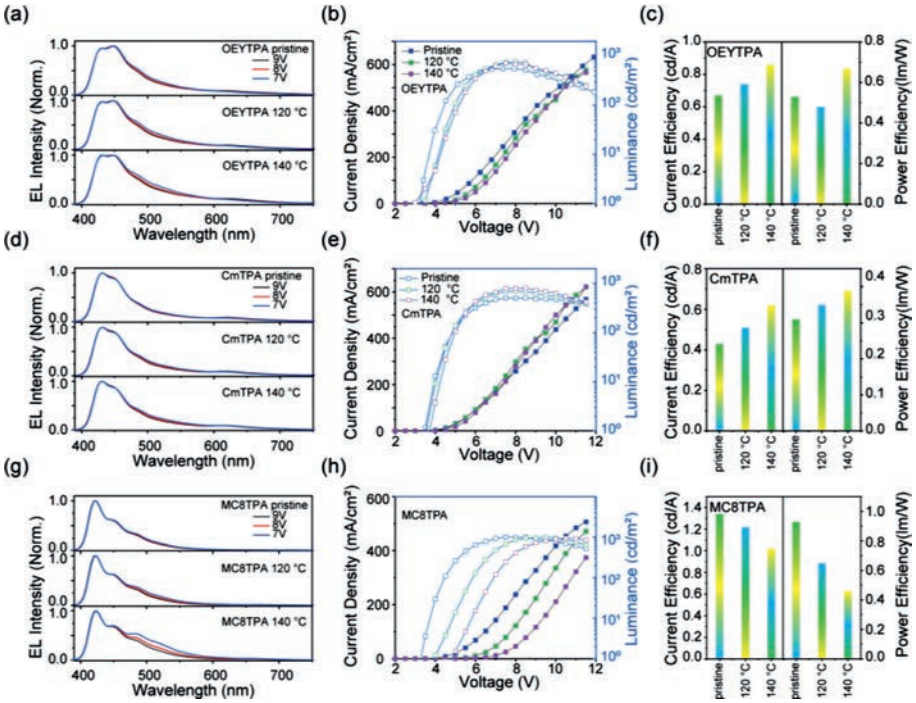

Fig. 6. Device performance of OEYTPA, CmTPA and MC8TPA-based OLEDs. (a, d, g) Electroluminescence (EL) spectra of devices based on OEYTPA, CmTPA and MC8TPA pristine film and annealed film (120 °C and 140 °C) after 2 h in the atmosphere. (b, e, h) Current Density-Voltage-Luminance (J-V-L) characteristics, and (c, f, i) Current and Power Efficiency *versus* Current Density curves for OLEDs devices.

ASE behavior also observed for MC8TPA after thermal annealing at 120 °C. However, there is a series of random lasing behavior with an extremely high threshold observed for annealed films obtained at 140 °C (Fig. 5d). Except for the emission property, optical microcavity is precondition to obtain random lasing [60]. It is effectively confirmed that micro- and nanoscale aggregate of MC8TPA are obtained in annealed film at high temperature (140 °C), similar to result of optical images (Fig. S10 in Supporting information). As we expected, both OEYTPA and CmTPA present considerable ASE behavior for pristine and annealed films. As displayed in Figs. 5b and c, the ASE thresholds were found to be 18.4 μJ/cm^2, 30.3 μJ/cm^2 and 34.8 μJ/cm^2, and 115.8 μJ/cm^2, 44.8 μJ/cm^2 and 50.5 μJ/cm^2 for OEYTPA and CmTPA pristine, annealed film obtained from 120 °C and 140 °C, respectively, comparable to the traditional light-emitting conjugated polymers [27–30,52,59,61–64]. Therefore, intermolecular side-chain coupling enable OEYTPA and CmTPA to present thermal-stable deep-blue emission behavior.

In recent decades, fluorene-based materials have been widely used for OLEDs due to their deep-blue emission and high luminance efficiency [39,65]. However, as presented in Fig. 3, discontinuous film morphology is negative to device performance and stability. In order to confirm this assumption, we fabricated a series of preliminary OLEDs based on three materials pristine and annealed films. Firstly, the highest occupied molecular orbital (HOMO) energy levels and lowest unoccupied molecular orbital (LUMO) energy levels of three materials were determined *via* cyclic voltammetry (CV). The Fc/Fc$^+$ redox were used as an internal standard to calibrate the oxidation potential of the materials and relevant data are listed in Fig. S11 and Table S3 (Supporting information). Therefore, the HOMO/LUMO energy levels estimated from the above equation are -5.14/-2.05, -5.14/-2.14 and -5.13/-2.11 eV for CmTPA, OEYTPA and MC8TPA, respectively. It exhibited that those HOMO energy levels of three compounds were slightly deeper than that of PEDOT: PSS which is -5.1 eV. Therefore, OLEDs devices were constructed with the configuration of ITO/poly(3,4-ethylenedioxy thiophene):poly(styrene sulfonicacid) (PEDOT:PSS) /emissive films/TMPyPB/LiF/Al. In order to evaluate the effect of thermal annealing on the device performance and stability, all emissive annealed films are obtained thermal treatment about 2 h in atmosphere.

Device performance of CmTPA, OEYTPA and MC8TPA-based OLEDs are displayed in Fig. 6 and Table S4 (Supporting information). The bulky steric units at 9-position of diarylfluorene molecules can effectively inhibit intermolecular aggregation, which ensure deep-blue emission. Similar to the corresponding PL spectra, all EL spectra of CmTPA, OEYTPA and MC8TPA pristine films consisted of two emitting peaks at 431 and 447 nm, respectively. No obvious green-band emission (550 nm) in two EL spectra of CmTPA and OEYTPA annealed films also confirmed the suppression of stronger intermolecular electron coupling of fluorene structures. The CIE coordinates for CmTPA and OEYTPA pristine films are about (0.19, 0.13) and (0.18, 0.13), respectively. More interestingly, the OLEDs fabricated from CmTPA and OEYTPA pristine film showed excellent EL spectral stability (Figs. 6a, d and g), with applied voltage increasing from 6 V to 9 V. Similarly, MC8TPA pristine film had a similar EL property. And, the EL spectra of OLED based on the MC8TPA annealed film exhibited three emission peaks at 432, 447 and 482 nm, respectively. However, weaker long-wavelength emission at 500–520 nm, are observed with increasing applied voltage from 6 V to 9 V, suggested residual physical defect emission. Corresponding CIE is changed from (0.16, 0.13) to (0.17, 0.15). Long-time thermal-annealing processing (2 h at 140 °C) may cause the intermolecular weaker aggregation for MC8TPA. Noted that MC8TPA films obtained under short annealed time (<10 min), had stable deep-blue emission. In a word, all OLEDs based on CmTPA and OEYTPA showed relative stable deep-blue EL property, confirmed the extremely weaker intermolecular aggregation in solid state after thermal treatment.

The device performances are displayed in Figs. 6b, e, h and c, f and i. It can be seen that the turn-on voltages (V_{on}) for the de-

vices based on MC8TPA pristine and annealed films are 3.3 V but increased to 4.8 V for annealed films, respectively. And the maximum current efficiency (CE) is decreasing from 1.34 cd/A (pristine) to 1.02 cd/A, reduced about 24% efficiency. Therefore, device efficiency is serious decreasing for MC8TPA after thermal annealing. We can also find that there is serious different current density and brightness verse voltage curves between devices based on pristine and annealed films, indicated the higher resistance of annealed film than pristine one, induced by the disruption of film morphology. On the other side, as displayed in Fig. 6, the device based on CmTPA and OEYTPA pristine and annealed film showed a similar current efficiency/brightness versus voltage curves, also indicated the similar film morphology, to ensure the stable electronic channel (Figs. 6b and e). More interestingly, the maximum CE of OLEDs based on the CmTPA and OEYTPA pristine film are calculated about 0.43 cd/A and 0.67 cd/A, and enhanced to about 0.62 cd/A and 0.85 cd/A, enhanced about 44% and 27%, respectively. Therefore, intermolecular coupling of CmTPA and OEYTPA in film states are positive to enhance emission spectral and device performance stability after thermal annealing.

In summary, we made a slight modification at the 4-position side chain end of fluorene, introducing active styryl double bond, so as to obtain a multi-molecules coupling, with similar thermal stability and luminescence stability for optoelectronic devices. Due to the intermolecular side-chain coupling, OEYTPA and CmTPA present an excellent morphological and emission spectral stability after annealing, compared to parent MC8TPA spin-coated film. Moreover, in contrary to the completely disruption of MC8TPA spin-coated film, CmTPA displayed an excellent stability after annealed films (obtained thermal treatment at 120 °C and 140 °C) secondary treatment under 160 °C in the air. As a result, OEYTPA and CmTPA annealed film obtained at 140 °C had an excellent ASE behavior with a maximum peak of 445 nm, but absent for MC8TPA film after thermal annealing at 140 °C. Finally, significantly different to low device stability of MC8TPA with a weaker green band emission, OLEDs based on CmTPA and OEYTPA annealed film displayed a higher device performance than pristine ones (enhanced about 47%). Therefore, combination of excellent charge-transport ability of TPA units, the intermolecular coupling strategy of a small molecular emitter will effectively improve its stability and emission behavior for solution-processing optoelectronic devices.

Declaration of competing interest

The authors declare that they have no known competing financial interests or personal relationships that could have appeared to influence the work reported in this paper.

Acknowledgments

The work was supported by the National Natural Science Foundation of China (Nos. 22075136, 61874053), National Key Research and Development Program of China (No. 2020YFA0709900), Natural Science Funds of the Education Committee of Jiangsu Province (No. 18KJA430009), Natural Science Foundation of Jiangsu Province (No. BK20200700), "High-Level Talents in Six Industries" of Jiangsu Province (No. XYDXX-019), Chain Postdoctoral Science Foundation (No. 2021M692623), the open research fund from State Key Laboratory of Supramolecular Structure and Materials (No. sklssm202108), Anhui Province Key Laboratory of Environment-friendly Polymer Materials and Anhui Province Key Laboratory of Optoelectronic Materials Science and Technology.

Supplementary materials

Supplementary data associated with this article can be found, in the online version, at doi:10.1016/j.cclet.2021.07.069.

References

[1] Y.G. Huang, E.L. Hsiang, M.Y. Deng, et al., Light Sci. Appl. 9 (2020) 105.
[2] M. Berggren, D. Nilsson, N.D. Robinson, Nat. Mater. 6 (2007) 3–5.
[3] J. Park, S. Heo, K. Park, et al., npj Flex. Electron. 1 (2017) 9.
[4] S.A. Veldhuis, P.P. Boix, N. Yantara, et al., Adv. Mater. 28 (2016) 6804–6834.
[5] Y.W. Xu, P. Xu, D.H. Hu, et al., Chem. Soc. Rev. 50 (2021) 1030–1069.
[6] M. Choi, B. Jang, W. Lee, et al., Adv. Funct. Mater. 27 (2017) 1606005.
[7] H. Zhang, J.A. Rogers, Adv. Opt. Mater. 7 (2019) 1800936.
[8] M. Karlsson, Z.Y. Yi, S. Reichert, et al., Nat. Commun. 12 (2021) 361.
[9] Z.H. Wei, K. Zhang, C.K. Kim, et al., Chin. Chem. Lett. 32 (2021) 493–496.
[10] X.K. Liu, W.D. Xu, S. Bai, et al., Nat. Mater. 20 (2021) 10–21.
[11] H. Zhang, K. Dasbiswas, N.B. Ludwig, et al., Nature 542 (2017) 328–331.
[12] L.H. Lan, J.H. Zou, C.B. Jiang, et al., Front. Optoelectron. 10 (2017) 329–352.
[13] A.J. Heeger, Chem. Soc. Rev. 39 (2010) 2354–2371.
[14] A. Kirch, A. Fischer, M. Liero, et al., Light Sci. Appl. 9 (2020) 5.
[15] X.T. Hao, L.J. McKimmie, T.A. Smith, J. Phys. Chem. Lett. 2 (2011) 1520–1525.
[16] M.N. Yu, H. Soleimaninejad, J.Y. Lin, et al., J. Phys. Chem. Lett. 9 (2018) 364–372.
[17] E. Ettedgui, G.T. Davis, B. Hu, et al., Synth. Met. 90 (1997) 73–76.
[18] Z.J. Liu, C.H. Lin, B.R. Hyun, et al., Light Sci. Appl. 9 (2020) 83.
[19] H.W. Chen, J.H. Lee, B.Y. Lin, et al., Light Sci. Appl. 7 (2018) 17168 -17168.
[20] A. Fischer, P. Pahner, B. Lüssem, et al., Phys. Rev. Lett. 110 (2013) 126601.
[21] C.J. Schaffer, C.M. Palumbiny, M.A. Niedermeier, et al., Adv. Mater. 25 (2013) 6760–6764.
[22] X. An, K. Wang, L.B. Bai, et al., J. Mater. Chem. C 8 (2020) 11631–11637.
[23] L.B. Bai, C. Sun, Y.M. Han, et al., Adv. Opt. Mater. 8 (2020) 1901616.
[24] Y.M. Han, L.B. Bai, M. Xu, et al., Adv. Opt. Mater. 8 (2020) 1902163.
[25] C. Pan, K. Sugiyasu, Y. Wakayama, et al., Angew. Chem. Int. Ed. 125 (2013) 10775–10779.
[26] F. Cacialli, J.S. Wilson, J.J. Michels, et al., Nat. Mater. 1 (2002) 160–164.
[27] Y.M. Han, C. Sun, L.B. Bai, et al., Phys. Status Solidi (RRL) Rapid Res. Lett. 14 (2020) 1900493.
[28] J.Y. Lin, G.Y. Zhu, B. Liu, et al., ACS Macro Lett. 5 (2016) 967–971.
[29] Q. Zhang, J.G. Liu, Q. Wei, et al., Adv. Funct. Mater. 28 (2018) 1705824.
[30] M.M. Mróz, G. Sforazzini, Y.C. Zhong, et al., Adv. Mater. 25 (2013) 4347–4351.
[31] M. Knaapila, A.P. Monkman, Adv. Mater. 25 (2013) 1090–1108.
[32] F.C. Spano, C. Silva, Ann. Rev. Phys. Chem. 65 (2014) 477–500.
[33] N. Sun, Y.Q. Liu, L.L. Sun, et al., J. Mater. Chem. C 8 (2020) 5064–5070.
[34] G. Méhes, C. Pan, F. Bencheikh, et al., ACS Macro Lett. 5 (2016) 781–785.
[35] F.X. Gu, H.K. Yu, P. Wang, et al., ACS Nano 4 (2010) 5332–5338.
[36] D.W. Bright, F.B. Dias, F. Galbrecht, et al., Adv. Funct. Mater. 19 (2010) 67–73.
[37] W.Y. Lai, Levell J.W., A.C. Jackson, et al., Macromolecules 43 (2010) 6986–6994.
[38] M.R. Craig, M.G. Hutchings, T.D.W. Claridge, et al., Angew. Chem. Int. Ed. 40 (2001) 1071–1074.
[39] L.H. Xie, C.R. Yin, W.Y. Lai, et al., Prog. Polym. Sci. 37 (2012) 1192–1264.
[40] S. Brovelli, F. Cacialli, Small 6 (2010) 2796–2820.
[41] Y.X. Li, S.S. Wang, Y. Yu, et al., Small 14 (2018) 1703151.
[42] D. Thomsson, R. Camacho, Y.X. Tian, et al., Small 9 (2013) 2619–2627.
[43] J.Y. Lin, B. Liu, M.N. Yu, et al., Adv. Mater. 31 (2019) 1804811.
[44] R. Noriega, J. Rivnay, K. Vandewal, et al., Nat. Mater. 12 (2013) 1038.
[45] X. Guo, A. Facchetti, Nat. Mater. 19 (2020) 922–928.
[46] H. Bronstein, C.B. Nielsen, B.C. Schroeder, et al., Nat. Rev. Chem. 4 (2020) 66–77.
[47] C.S. Li, R.S. Nobuyasu, Y.K. Wang, et al., Adv. Opt. Mater. 5 (2017) 1700435.
[48] M. Singh, H.M. Haverinen, P. Dhagat, et al., Adv. Mater. 22 (2010) 673–685.
[49] M. Berggren, D. Nilsson, N.D. Robinson, Nat. Mater. 6 (2007) 3–5.
[50] Y.M. Han, L.B. Bai, C.R. Yin, et al., J. Mater. Chem. C 5 (2017) 9903.
[51] L.B. Bai, Z. Wang, Y.M. Han, et al., Nano Energy 46 (2018) 241–248.
[52] C.J. Ou, C. Zhu, X.H. Ding, et al., J. Mater. Chem. C 5 (2017) 5345–5355.
[53] W. Cho, S.S. Reddy, J. Kim, et al., J. Mater. Chem. C 6 (2018) 11714–11721.
[54] M. Auer, L. Pevzner, S. Sax, et al., Supramol. Mater. Opto-Electron. 7 (2015) 226–272.
[55] C.Y. Lin, Y.C. Lin, W.Y. Hung, et al., J. Mater. Chem. 19 (2009) 3618–3623.
[56] K.Y. Zhou, H.F. Pan, Y.J. Zhang, et al., Org. Biomol. Chem. 18 (2020) 3754–3760.
[57] H.L. Dong, W.P. Hu, Acc. Chem. Res. 49 (2016) 2435–2443.
[58] C.J. Ou, N.J. Cheetham, J.N. Weng, et al., iScience 16 (2019) 399–409.
[59] C. Sun, M.M. Mróz, J.R.C. Smirnov, et al., J. Mater. Chem. C 6 (2018) 6591–6596.
[60] A. Tulek, R.C. Polson, Z.V. Vardeny, Nat. Phys. 6 (2010) 303–310.
[61] L.B. Bai, B. Liu, Y.M. Han, et al., ACS Appl. Mater. Interfaces 9 (2017) 37856–37863.
[62] B. Liu, J.Y. Lin, F. Liu, et al., ACS Appl. Mater. Interfaces 8 (2016) 21648–21655.
[63] E.B. Namdas, M.H. Tong, P. Ledochowitsch, et al., Adv. Mater. 21 (2010) 799–802.
[64] M. Xu, M.N. Yu, B. Liu, et al., Cell Rep. Phys. Sci. 1 (2020) 100029.
[65] L.H. Xie, S.H. Yang, J.Y. Lin, et al., Philos. Trans. 371 (2013) 20120337.